8. Georgii, H.-O. (1999): 'Translation invariance and continuous symmetries in two-dimensional continuum systems'. In: *Mathematical results in Statistical Mechanics*, ed. by S. Miracle-Sole, J. Ruiz, V. Zagrebnov (World Scientific, Singapore etc.), pp. 53–69
9. Georgii, H.-O., O. Häggström (1996): 'Phase transition in continuum Potts models', *Commun. Math. Phys.* **181**, pp. 507–528
10. Georgii, H.-O., O. Häggström, C. Maes (1999): 'The random geometry of equilibrium phases'. In: *Critical phenomena*, ed. by Domb and J.L. Lebowitz (Academic Press), forthcoming
11. Georgii, H.-O., Y. Higuchi (1999): 'Percolation and number of phases in the 2D Ising model', submitted to *J. Math. Phys.*
12. Georgii, H.-O., T. Küneth (1997): 'Stochastic comparison of point random fields', *J. Appl. Probab.* **34**, pp. 868–881
13. Grimmett, G.R. (1999): *Percolation*, 2nd ed. (Springer, New York)
14. Gruber, Ch., R.B. Griffiths (1986): 'Phase transition in a ferromagnetic fluid', *Physica A* **138**, pp. 220–230
15. Häggström, O., M.N.M. van Lieshout, J. Møller (1997): 'Characterization results and Markov chain Monte Carlo algorithms including exact simulation for some spatial point processes', *Bernoulli*, to appear
16. Likos, C.N, K.R. Mecke, H. Wagner (1995): 'Statistical morphology of random interfaces in microemulsions', *J. Chem. Phys.* **102**, pp. 9350–9361
17. Mecke, K.R. (1996): 'A morphological model for complex fluids', *J. Phys.: Condens. Matter* **8**, pp. 9663–9668
18. Meester, R., R. Roy (1996): *Continuum Percolation* (Cambridge University Press)
19. Penrose, M.D. (1991): 'On a continuum percolation model', *Adv. Appl. Probab.* **23**, pp. 536–556
20. Swendsen, R.H., J.-S. Wang (1987): 'Nonuniversal critical dynamics in Monte Carlo simulations', *Phys. Rev. Lett.* **58**, pp. 86–88
21. Thönnes, E. (1999): 'Perfect simulation of some point processes for the impatient user', *Adv. Appl. Probab.* **31**, pp. 69–87
22. Widom, B., J.S. Rowlinson (1970): 'New model for the study of liquid-vapor phase transition', *J. Chem. Phys.* **52**, pp. 1670–1684

Fun with Hard Spheres

Hartmut Löwen

Institut für Theoretische Physik II, Heinrich-Heine-Universität Düsseldorf,
Universitätsstraße 1
D-40225 Düsseldorf, Germany

Abstract. Thermostatistical properties of hard sphere and hard disk systems are discussed. In particular we focus on phase transitions such as freezing in the thermodynamic limit. Results based on theory and computer simulations are given. It is emphasized that suspensions of sterically-stabilized colloids represent excellent realizations of the hard sphere model. Finally a survey of current research activities for hard sphere systems is presented and some recent results are summarized.

1 Motivation

This article aims at several points: First, it is a brief introduction to classical statistical physics of hard sphere-like systems ranging from elementary definitions to recent research activities. In this respect it represents both a tutorial and a review. Second, it is written by a physicist, not by a mathematician. This implies that emphasis is put on simple physical pictures omitting any mathematical rigour. However, it is tried to link to the literature of mathematical physics and to establish thereby a connection between physics and mathematics. Third, if possible, relations between statistical physics and geometry are discussed.

2 Introduction: The Model

The hard sphere model is defined by a pair interaction between two classical particles that only involves a non-overlap condition. The potential energy of a pair of hard spheres is

$$V(r) = \begin{cases} \infty \text{ if } r < \sigma \\ 0 \quad \text{else} \end{cases} \tag{1}$$

where σ is the diameter of the spheres and r is the distance between the two centers of the spheres, see Fig. 1 on page 315. The potential $V(r)$ is sketched in Fig. 2. It is very "steep" for touching spheres. More formally, the peculiarity of the hard sphere (or any other hard body) potential is that it sets a length scale (namely σ) but it does not set any energy scale. Clearly, a configuration of two overlapping spheres is punished by an infinite energy. Having a Boltzmann factor in mind, this implies that such overlapping configurations do not occur, i.e., they have no statistical weight in a thermal average. If one sphere is fixed, a second sphere can possess any center position except for a sphere around the first sphere with a *radius* σ. This is the reason why one calls the potential (1) an "excluded volume" interaction.

Interesting questions and non-trivial effects arise when many hard spheres are interacting at high density. To be specific we consider N hard spheres in a system volume Ω at a temperature T. The particle number density is then

$$\rho = N/\Omega \tag{2}$$

An equivalent dimensionless measure of the number density is provided by the so-called *packing fraction* (or volume fraction) η which is the ratio of the volume of the N spheres and the total accessible volume Ω:

$$\eta = N\Omega_s/\Omega = \pi\rho\sigma^3/6 \tag{3}$$

where $\Omega_s = \pi\sigma^3/6$ is the volume of a single sphere.

Let the set of three-dimensional vectors $\{\boldsymbol{R}_1, \boldsymbol{R}_2, ..., \boldsymbol{R}_N\}$ denote an arbitrary configuration of N spheres, see Fig. 3. Then the total potential energy associated to this configuration is

$$V(\boldsymbol{R}_1, \boldsymbol{R}_2, ..., \boldsymbol{R}_N) = \sum_{i,j=1;i<j}^{N} V(|\boldsymbol{R}_i - \boldsymbol{R}_j|) \tag{4}$$

where we distinguish different functions by giving them different arguments. Obviously, as $V(\boldsymbol{R}_1, \boldsymbol{R}_2, ..., \boldsymbol{R}_N)$ is a sum over hard sphere potentials, it only takes the two values 0 and ∞. Consequently, for the Boltzmann factor, we get

$$\exp(-\beta V(\boldsymbol{R}_1, \boldsymbol{R}_2, ..., \boldsymbol{R}_N)) \equiv \exp(-V(\boldsymbol{R}_1, \boldsymbol{R}_2, ..., \boldsymbol{R}_N)) \tag{5}$$

with $\beta = 1/k_BT$, k_B denoting Boltzmann's constant. This implies that the temperature scales out trivially. Or, in other words, hard objects are *athermal*; all their structural and thermodynamical properties do not depend on temperature so that the density ρ (or the packing fraction η) is the only relevant thermodynamical variable. The only relevance of temperature is that k_BT sets the natural energy scale. This can directly be seen by defining the classical canonical partition function

$$Z = \frac{1}{\Lambda^{3N}N!}\int_\Omega d^3R_1 ... \int_\Omega d^3R_N \exp(-V(\boldsymbol{R}_1, \boldsymbol{R}_2, ..., \boldsymbol{R}_N)) \tag{6}$$

Here, the de Broglie thermal wave-length Λ is just an arbitrary length scale to make the partition function dimensionless. Λ is irrelevant since multiplying Λ by a scaling factor simply means that the chemical potential μ is shifted by an (irrelevant) constant (the definition of μ is given later, see (27) and [18]). In (6), the factor $1/N!$ avoids multiple counting of configurations that arise simply from interchanging particle labels. Then the classical canonical (Helmholtz) free energy is

$$F = -k_BT \ln Z \tag{7}$$

from which we can extract all information required for equilibrium thermodynamics. Here, it becomes again evident that the thermal energy k_BT simply sets the energy scale of the Helmholtz free energy but the reduced quantity F/k_BT is independent of temperature.

Interesting collective phenomena are conveniently studied in the so-called thermodynamic limit (TDL) where the number of particles, N, and the system volume, Ω, become infinite such that the particle number density $\rho = N/\Omega$ stays finite. A phase transition is signalled by a nonanalytical dependence of the Helmholtz free energy on the thermodynamic parameters such as density ρ and temperature T. The non-analyticities determine the phase diagram of the system. At this stage we shall not study the existence of the thermodynamic limit but simply take it for granted. Unfortunately the thermodynamic limit implies many integrations in (6) for the partition function Z. Hence one has either to rely on Monte Carlo techniques to evaluate this high-dimensional integral or to perform approximation methods. As far as I know, there is no exact solution for a phase transition in D-dimensional hard sphere systems if D is larger than 1, for a more detailed discussion see below.

One can also add an *external potential* $V_{ext}(\boldsymbol{r})$ to the system. If $V_{ext}(\boldsymbol{r})$ vanishes, one speaks about a bulk system. The presence of an external potential means that the total potential energy now reads

$$V(\boldsymbol{R}_1, \boldsymbol{R}_2, ..., \boldsymbol{R}_N) = \sum_{i=1}^{N} V_{ext}(\boldsymbol{R}_i) + \sum_{i,j=1;i<j}^{N} V(|\boldsymbol{R}_i - \boldsymbol{R}_j|) \tag{8}$$

Typical examples for sources of an external potential are system walls and system boundaries, a gravitational field, external laser-optical fields etc. For a fixed external potential one can also perform the thermodynamic limit. In cases of a symmetry-breaking phase transition, one can force the system to be in a symmetry-broken phase by imposing a suitable external potential $V_{ext}(\boldsymbol{r}) = \epsilon f(\boldsymbol{r})$. Now the sequence of the TDL and the limit $\epsilon \to \infty$ is crucial and interchanging both leads to different results. While one always gets a homogeneous bulk system if the limit $\epsilon \to \infty$ is performed first, a symmetry-broken state may be reached if the limit $\epsilon \to \infty$ is performed after the TDL.

One basic question concerns the problem of close-packing in the TDL: A first part of the problem addresses the maximum of the packing fraction which defines the socalled close-packed fraction η_{cp}. The second part is the corresponding close-packed configuration which leads to this close-packed density. Physicists have assumed over centuries that the close-packed situation of spheres is a stack of intersecting two-dimensional triangular lattices. This gives

$$\eta_{cp} = \pi/3\sqrt{2} = 0.740... \tag{9}$$

In fact, a rigorous mathematical proof for this was lacking until 1998 when Hales discovered one (see e.g. [19]). The problem was that locally one can achieve closer packings by icosahedral structures but these packings cannot be joint

together to fill the whole space. In fact, it is much simpler to prove that $\eta_{cp} = \pi/3\sqrt{2}$ among all periodic lattice structures which was done in 1831 by Gauss. See the contribution of J. Wills in this volume for different problems of close-packing. It is clear that there are many configurations leading to the same close-packed fraction η_{cp}, or, in other words, there is a high *degeneracy* of close-packed configurations. In one of them, the spheres are sitting on face-centered-cubic (fcc) lattice positions which corresponds to a stacking sequence $ABCABC...$. Another structure is the hexagonal-close-packed (hcp) lattice corresponding to a stacking sequence $ABAB...$. A more exotic structure is the double hcp lattice with a stacking sequence $ABACABAC...$, but also a random stacking sequence as $ABCBACBABCA...$ is conceivable.

One may now look for a phase transition in the range of intermediate densities $0 < \eta < \eta_{cp}$. In fact, it is by now well-established and accepted that hard spheres exhibit a freezing transition which we shall discuss in detail in chapter 3 and 4.

Let us finish with two more general remarks on the hard sphere model: First, due to its temperature-independence, it is the simplest non-trivial model for an interaction. In this sense, it is useful as a reference system for systems with more complicated interactions and particle shapes. Since a theoretical physicist typically first tries to incorporate the essential ingredients in a simple model in order to study the principle mechanisms, the hard sphere model is the first choice of a reasonable approximation. This is illustrated in the cartoon of Fig. 4: if a theoretician studies a herd of elephants, his first thought is to approximate them by hard spheres neglecting any details (trunks, tails, etc.). On a length scale compatible with the overall size of an eliphant this approximation is not completely ridiculous!

The second important fact is that the equilibrium thermodynamical properties of the hard sphere model can actually be probed in nature by examining suspensions of spherical sterically-stabilized colloidal particles (for a review, see [75]). Such particles have a mesoscopic size between $1nm$ and $1\mu m$. They are coated by polymer brushes and suspended in a microscopic solvent. A schematic picture is given in Fig. 5. A typical colloidal material is polymethylmethacrylate (PMMA). The omnipresent van-der-Waals attraction between two colloidal particles can be tuned to be extremely small by "index-matching" the particles. If the typical length ℓ of the adsorbed polymer brushes is much smaller than the diameter σ of the colloidal spheres, the total interaction between the particles is dominated by excluded-volume effects. This enables one to directly compare experimental data with predictions from the hard-sphere model. An electron-micrograph of colloidal particles is shown in Fig. 6. Indeed one sees that all the spheres have the same diameter, i.e. the socalled size-polydispersity is small. Still, in an actual quantitative comparison, there are three caveats: i) Is the size-polydisperity really small in the samples? ii) Are the colloidal particles really spherical i.e. isotropic? iii) Are the interactions stiff or is there still a penetrability of spheres? In recent experiments it has been proved that all these possible problems can be avoided by carefully "cooking" the suspensions [75].

3 The Hard Sphere Model in Arbitrary Spatial Dimension

3.1 General

It is instructive to generalize the hard sphere model to an arbitrary spatial dimension D. The reason to do so is twofold: First, one can formally embed the three-dimensional case in a general context. Second, in some special spatial dimensions, exact results are available.

The interaction between two hard "hypersphere" in spatial dimension D is

$$V(|\boldsymbol{r}|) = \begin{cases} \infty \text{ if } |\boldsymbol{r}| < \sigma \\ 0 \quad \text{else} \end{cases} \tag{10}$$

Here, $\boldsymbol{r} = (r_1, r_2, ..., r_D)$ is a D-dimensional position vector and $|\boldsymbol{r}| = \sqrt{\sum_{i=1}^{D} r_i^2}$ is the distance between the centers of two hyperspheres. It is straightforward to generalize the formalism developed in the last chapter to arbitrary D. The canonical partition function now is

$$Z = \frac{1}{\Lambda^{DN} N!} \int_\Omega d^D R_1 ... \int_\Omega d^D R_N \cdot \exp(-V(\boldsymbol{R}_1, \boldsymbol{R}_2, ..., \boldsymbol{R}_N)) \tag{11}$$

where $\boldsymbol{R}_i$ now is the D-dimensional position vector of the ith particle. Let us subsequently discuss some special cases.

3.2 One-Dimensional Case

In the *one-dimensional case* ($D = 1$) we are dealing with N hard rods of width σ on a line of length L, see Fig. 7. Here the number "line" density is $\rho = N/L$ and the packing fraction is simply $\eta = \rho\sigma$. The close-packed situation is trivial in this case leading to $\eta_{cp} = 1$. This case is remarkable insofar as the partition function Z and the Helmholtz free energy F can be calculated analytically even in the thermodynamic limit. This was done by Tonks [83] in the early days of statistical mechanics. The final result for the reduced Helmholtz free energy per particle is

$$\frac{F}{k_B T N} = \ln(\rho\Lambda) - 1 - \ln(1 - \rho\sigma) \tag{12}$$

As a result, there is no phase transition as F is analytic in the particle density ρ in the domain $0 < \rho < 1/\sigma$. The only nonanalyticity occurs at the boundaries for $\rho \to 1/\sigma$ (close-packing) where F diverges to infinity as all rods are forced to touch each other. But this is not a true phase transition.

3.3 Two-Dimensional Case

In the *two-dimensional case* ($D = 2$) of hard disks the close-packed area fraction is $\eta_{cp} \equiv \pi\rho_{cp}\sigma^2/4 = \pi/2\sqrt{3} = 0.907...$ corresponding to a perfect triangular lattice with long-ranged translational order. The proof is attributed to Lagrange who did it as early as in 1773. Note that apart from trivial translations, there is no degeneracy as in the three-dimensional case. As far as phase transitions are concerned, no rigorous result is known so far. The Fröhlich-Pfister argument for the absence of long-ranged translational order [35] is not possible for hard disks as some smoothness conditions are required for the mathematical proof which are not fulfilled for hard disks. The nature of the freezing transition for hard disks is still debated in recent literature [49,60] but at least there is evidence from computer simulations for a freezing transition into a triangular lattice occuring for a density well-separated from close-packing. Most probably the transition is in accordance with the Kosterlitz-Thouless scenario [49].

3.4 Arbitrary Dimension

Situations of hyperspheres with $D > 3$ are also conceivable, at least formally. If one restricts the consideration within periodic lattice types, the close-packed density is known for $D = 4, 5, 6, 7, 8$ and only for peculiar higher dimensions but not in general, see [55] for a compilation of recent data. Apart from very recent work [30], I am not aware of any investigation of phase transitions in higher dimensions.

3.5 Degenerate Cases

Finally let us discuss two "degenerate" situations, namely $D = 0$ and the limit $D \to \infty$. The zero-dimensional case can be viewed as a sphere in a cavity that holds only one particle. In this case one can compute the partition function exactly, of course. This limiting case is important to check the validity of different density functional approximations. The limit of infinite dimension is more tricky. There are bounds for the close-packed density proved at the beginning of this century by Minkowski and by Blichfeld (in [55]). In fact, one knows

$$\frac{\zeta(D)}{2^{D-1}} \leq \eta_{cp} \leq \frac{D+2}{2} 2^{-D/2} \tag{13}$$

where $\zeta(D)$ denotes the Riemannian zeta-function. This implies that the close-packed density vanishes in the limit $D \to \infty$. A virial analysis shows that only the first and the second virial coefficients survive in the limit $D \to \infty$ such that one can use an Onsager-type analysis to extract the instability of the fluid, see [32, 33] and [89]. The rigorous location of the freezing which should also depend on the structure of the crystalline phase is still an open question. However there are recent investigations using diagrammatic expansions [34]. The question might be easier to answer for parallel hard hypercubes where the problem of close-packing is trivial and an instability analysis suggest a second-order transition from a fluid phase into a hypercubic lattice [50].

4 Hard Spheres and Phase Transitions: Theory

In this chapter we review some popular theories for the many-body hard sphere system. Most theories are constructed in such a way that they only work in a certain phase. The easiest theory which applies to the solid phase is the cell or "free volume" approach. We also mention the Percus-Yevick and scaled-particle theory which describes the fluid state. Finally a unifying theory which works in both phases can be obtained by exploiting the density functional technique.

4.1 Intuitive Arguments

Why is there a fluid-solid transition in the hard sphere system? This is not obvious at all from intuition and it is still not accepted by everybody in the physics community. In order to discuss this further, we stress that the averaged potential energy vanishes, i.e.

$$< V(\boldsymbol{R}_1, \boldsymbol{R}_2, ..., \boldsymbol{R}_N) >= 0 \tag{14}$$

as configuration where spheres are at contact have zero statistical weight. Here $< A >$ denotes the canonical average of the quantity A

$$< A > \; = \frac{1}{Z\Lambda^{3N}N!} \cdot \int_\Omega d^3R_1 \; ... \int_\Omega d^3R_N \; A \; \exp(-V(\boldsymbol{R}_1, \boldsymbol{R}_2, ..., \boldsymbol{R}_N)) \tag{15}$$

This immediately implies that the total free energy can be written as

$$F = \bar{H}_{kin} - TS = \frac{3}{2} N k_B T - TS \tag{16}$$

where $\bar{H}_{kin} = 3Nk_BT/2$ is the averaged kinetic energy of the spheres and S is the entropy. Hence, apart from the trivial constant $\frac{3}{2}Nk_BT$, there is only entropy. This is the reason why one says that hard spheres are an *entropic* system. The intuitive feeling is that high entropy means low order. According to this intuition, an ordered phase should have a lower entropy or a higher free energy than a disordered phase. Hence a disordered phase has minimal free energy and should be the thermodynamically stable phase. This simple argument, however, is wrong. In fact, at high densities, the entropy of hard spheres is smaller in the ordered (solid) phase than in the disordered (fluid) phase! A more refined argument splits the entropy into two different parts which is visualized for hard disks in Fig. 8. For any random or disordered situation, one has many possible configurations but as the density grows more and more of these configurations are blocked by touching nearest neighbours. In an ordered solid-like phase, on the other hand, there is only one basic lattice configuration possible, but one can generate further non-overlapping configurations by moving the disks slightly away form their lattice position. Hence, a fluid phase has a high

configurational entropy but a small "free volume" entropy, while a solid phase has a low configurational entropy but a high correlational (or "free volume") entropy. Both kind of entropies depend on the density. The configurational entropy is dominating for small densities whereas the "free volume" entropy is dominating near close-packing. Consequently there has to be a phase transition between these two situations for intermediate densities. It has to be emphasized that the freezing transition is not driven by competition between potential energy and entropy but by competition between these two different kinds of entropies. This is even the generic mechanism for freezing which also works for soft repulsive potentials. We finally remark that these two different kinds of entropies can be properly defined and calculated by density functional theory [9].

4.2 The Cell Model

The cell theory or free volume approach (for a general introduction and historical remarks see [61]) starts from a given hard sphere solid. We now draw the Wigner-Seitz (or Voronoi) cells of this lattice, see Fig. 9. Let us assume that each sphere can move freely only within its own Wigner-Seitz cell. Obviously we are neglecting some further configurations by this restriction, therefore this theory clearly is an approximation. But this approximation should be justified near close-packing. Equivalently, this means that any center of the spheres can move within a small "free volume" Ω_f which has the same form as the Wigner-Seitz cell, see again Fig. 9. By counting the configurations and considering trivial particle exchanges we estimate the partition function as follows:

$$Z \geq Z_{CT} = \frac{1}{\Lambda^{3N}} \Omega_f^N \tag{17}$$

and the free energy is

$$\frac{F}{k_B T N} \leq \frac{F_{CT}}{k_B T N}$$
$$= \ln \sqrt{2} + 3 \ln(\Lambda/\sigma) - 3 \ln[(\frac{\pi\sqrt{2}}{6\eta})^{1/3} - 1] \tag{18}$$

The cell theory thus establishes a rigorous upper bound to the free energy. Clearly, the free energy diverges as $\eta \to \eta_{cp}$. The leading logarithmic divergence becomes in fact asymptotically exact as $\eta \to \eta_{cp}$ [61]. In the one-dimensional case ($D = 1$) the cell theory gives the exact equation of state which is the pressure

$$P = -\frac{\partial F}{\partial \Omega}|_{N,T} \tag{19}$$

as a function of density, but the free energy itself is not exact.

4.3 Percus-Yevick Theory

Another obvious approach is to start from very low densities where the system is an ideal gas and calculate perturbatively the next leading corrections. The

equation of state can be expressed in powers of the density. Clearly the starting point here is the fluid phase. It is known that the virial expansion has a finite radius of convergence in the density for any spatial dimension D [53] but the actual convergence radius might be much larger. One could surmise that all the virial coefficients are positive but a rigorous mathematical proof is still lacking.

The virial expansion can be improved by solving socalled liquid-integral equations [41]. In fact the following Percus-Yevick closure relation has been found to give good result even for intermediate packing fractions up to $\eta \approx 0.3$. The closure is expressed in terms of two correlation functions. The first is the *pair distribution function* $g(r)$ defined as

$$g(r) = \frac{1}{\rho N} < \sum_{i,j=1;i<j}^{N} \delta(\boldsymbol{r} - (\boldsymbol{R}_i - \boldsymbol{R}_j)) > \tag{20}$$

This function gives the probability of finding a particle at distance r from a given fixed particle. A typical $g(r)$ for hard spheres is shown in Fig. 10. For $r < \sigma$, $g(r)$ vanishes which is just the non-overlap condition:

$$g(r) = 0 \quad \text{for} \quad r < \sigma \tag{21}$$

For $r \to \infty$, $g(r)$ is normalized to 1. For very small densities, $g(r) = \Theta(r - \sigma)$ where $\Theta(x)$ denotes the unit step function while for large densities, $g(r)$ exhibits a structure from neighbouring shells of particles. At very high densities $\eta \approx 0.5$, the contact value $g(r \to \sigma^+) \equiv g(\sigma^+)$ increases to large values and the second neighbour shell becomes split exhibiting a shoulder [84], see Fig. 10, which is in accordance with confocal microscopy measurements on sterically-stabilized colloidal suspensions [85]. The pair correlation function is also discussed in the contribution of Döge et al. in this volume. The equation of state can exactly be related [41] to the contact value of $g(r)$ by using the virial expression:

$$\frac{P}{\rho k_B T} = 1 + 4\eta g(\sigma^+) \tag{22}$$

So once one knows $g(\sigma^+)$ for any density one gets F by integrating (22).

The second correlation function is the Ornstein-Zernike or *direct correlation function*. It is implicitly defined via the Ornstein-Zernike relation

$$g(r) - 1 = c(r) + \rho \int d^3r' (g(r') - 1) c(|\boldsymbol{r} - \boldsymbol{r}'|) \tag{23}$$

The Percus-Yevick closure combines the exact relation (21) with the approximation

$$c(r) = 0 \quad \text{for} \quad r > \sigma \tag{24}$$

The advantage of the Percus-Yevick theory is that it can be solved analytically for $c(r)$. Using the Ornstein-Zernike relation and the virial expression one can

deduce an analytical form for the Helmholtz free energy as follows

$$\frac{F}{k_BTN} \approx \frac{F_{PY}}{k_BTN} = 3\ \ln(\Lambda/\sigma) - 1 + \ln(6\eta/\pi) - \ln(1-\eta) + \frac{3}{2}[\frac{1}{(1-\eta)^2} - 1] \quad (25)$$

This expression clearly diverges when $\eta \to 1$ being an artifact of the approximation which is meant only for small η. Finally we remark that the Percus-Yevick direct correlation function and the free energy are exact in one spatial dimension.

4.4 Estimation of the Freezing Transition

Knowing analytical expressions (18) and (25) for the free energy in the solid and fluid state, we can estimate the location of the freezing transition. There are three conditions for phase coexistence. The first concerns thermal equilibrium, i.e. the temperature in the two coexisting phases has to be equal, $T_1 = T_2$. Due to the trivial temperature dependence of the free energy for hard sphere, this condition is fulfilled. Second, the pressure in the two coexisting phases has to coincide, $P_1 = P_2$, (mechanical equilibrium). Third, chemical equilibrium requires the same chemical potential in the two coexisting phases, $\mu_1 = \mu_2$. The latter two conditions are equivalent to Maxwell's common-tangent construction. This is easily explained in terms of the free energy per volume $f_i = F_i/V = f_i(T,\rho)$ of the two phases ($i = 1, 2$). The two pressures and chemical potentials can be written as

$$P_i = -\frac{\partial F_i}{\partial \Omega}|_{T,N} = f_i - \rho_i \frac{\partial f_i(T, \rho = \rho_i)}{\partial \rho}|_T \quad (26)$$

and

$$\mu_i = \frac{\partial F_i}{\partial N}|_{T,\Omega} = \frac{\partial f_i(T, \rho = \rho_i)}{\partial \rho}|_T \quad (27)$$

where $i = 1, 2$ labels the two different phases. The two conditions $P_1 = P_2$ and $\mu_1 = \mu_2$ hence are expressed as

$$f_1'(\rho_1) = f_2'(\rho_2) \quad (28)$$

and

$$f_2(\rho_2) = f_1(\rho_1) + f_1'(\rho_1)(\rho_2 - \rho_1) \quad (29)$$

with $f_1'(\rho) \equiv \partial f_i/\partial\rho|_T$. These equations mean that one finds the two coexisting densities ρ_1 and ρ_2 by a common tangent construction for the two free energy densities plotted as a function of density. In our case of hard sphere freezing this is visualized in Fig. 11. Assuming that the cell theory (solid line in Fig. 11) and the Percus-Yevick expression (dashed line in Fig. 11) are valid for any density the Maxwell common tangent construction leads to coexisting packing fractions of $\eta_f = 0.57$ for the fluid phase and $\eta_s = 0.65$ for the solid phase. Of course, actual data for free energies are required for intermediate densities where the two theoretical expressions are expected to fail. Nevertheless, we shall see later

that the coexisting densities and the relatively large density jump across the transition are in fairly good agreement with "exact" computer simulations.

These considerations also give a clue of how to prove rigorously the existence of the freezing transition. The solid cell model gives an *upper bound* to the free energy in the solid phase. If one would know a *lower bound* of the free energy in the fluid phase and could show that this lower bound hits the upper bound of the cell model, then the existence of the phase transition would be proven. The construction of a lower bound in the fluid phase is strongly linked to the virial coefficients which determine the convergence of the virial expansions in powers of the density. If all the virial coefficients would be positive, then there has to be a freezing transition. Even if only the virial expansion truncated after the second coefficient would be a lower bound, then it hits the solid cell theory for spatial dimensions $D > 8$ [30]. However, although all these assumptions seem to be plausible for physicists, they need to be proved mathematically. Therefore, to establish rigorously the exostence of the freezing transition is still an open unsolved problem.

4.5 Scaled Particle Theory

The scaled particle theory ([76]; for a review see [8]) considers the reversible work to create a spherical cavity of radius R_0 in a hard sphere fluid. Formally the cavity can be regarded as a further "scaled" particle. One knows the relation of this work to the bulk pressure for the special case $R_0 = 0$. For $R_0 \to \infty$, this work is connected to the interfacial free energy γ between a planar hard walls and a hard sphere fluid. Interpolating between these special cases one gets the work for $R_0 = \sigma$ from which one deduces the contact value $g(\sigma^+)$. Using the exact virial expression (22), one gets the free energy. Remarkably, though a completely different phyical picture is used, the scaled-particle results coincides with the Percus-Yevick virial expression (25). The scaled-particle theory cannot be applied to the solid but it has the advantage that it can be generalized to hard convex bodies with non-spherical shapes as e.g. hard spherical-capped cylinders.

4.6 Density Functional Theory

Density functional theory (DFT) provides a unified picture of the solid and fluid phase. In fact as we shall show below, it is a way to combine the cell theory for the solid with the Percus-Yevick (or scaled particle) theory of the liquid. As for general reviews, see e.g. [57] and [29]. The cornerstone of DFT is the Hohenberg-Kohn-Sham theorem which was generalized to finite temperatures by Mermin. It guarantees the existence of a functional for the excess free energy $\mathcal{F}_{exc}[\rho]$ of the (in general inhomogeneous) one-particle density $\rho(\boldsymbol{r})$. This functional has the unique property that the functional for the grandcanonical free energy

$$\tilde{\Omega}[\rho] := \mathcal{F}_{exc}[\rho] + \int_\Omega d^3r\rho(\boldsymbol{r})\{V_{ext}(\boldsymbol{r}) - \mu - 1 + k_BT\ln(\Lambda^3\rho(\boldsymbol{r}))\} \quad (30)$$

is minimized by the equilibrium one-particle density

$$\rho_0(\boldsymbol{r}) =< \sum_{i=1}^{N} \delta(\boldsymbol{r} - \boldsymbol{R}_i) > \tag{31}$$

and the minimum $\bar{\Omega}[\rho_0(\boldsymbol{r})]$ is the actual grandcanonical free energy which is equal to $-P\Omega$ in the bulk case. The problem, however, is that nobody knows the actual form of the functional $\mathcal{F}_{exc}[\rho]$. It is only for the trivial case of an (non-interacting) ideal gas that $\mathcal{F}_{exc}[\rho]$ is known to vanish.

Different approximations for $\mathcal{F}_{exc}[\rho]$ designed for strongly interacting systems (in particular for hard spheres) are on the market. Most of them make use of the fact that the direct (Ornstein-Zernike) correlation function introduced in chapter 3.3 is the second functional derivative of $\mathcal{F}_{exc}[\rho]$ in the homogenous bulk fluid [41]:

$$c(|\boldsymbol{r}_1 - \boldsymbol{r}_2|) = \frac{1}{k_B T} \frac{\delta^2 \mathcal{F}_{exc}}{\delta\rho(\boldsymbol{r}_1)\delta\rho(\boldsymbol{r}_2)}|_{hom} \tag{32}$$

The most elaborated and reliable functional for hard spheres is that recently developed by [79]. It is fixed by approximating

$$\mathcal{F}_{exc}[\rho] \approx k_B T \int_\Omega d^3 r \Phi[\{n_\alpha(\boldsymbol{r})\}] \tag{33}$$

where one introduced a set of weighted densities

$$n_\alpha(\boldsymbol{r}) = \int_\Omega d^3 r' \rho(\boldsymbol{r}') w_\alpha(\boldsymbol{r} - \boldsymbol{r}') \tag{34}$$

Here, the index $\alpha = 0, 1, 2, 3, V1, V2$ labels six different weighted densities and six different associated weight functions. Explicitly these six weight functions are given by

$$w_0(\boldsymbol{r}) = \frac{w_2(\boldsymbol{r})}{\pi\sigma^2} \tag{35}$$

$$w_1(\boldsymbol{r}) = \frac{w_2(\boldsymbol{r})}{2\pi\sigma} \tag{36}$$

$$w_2(\boldsymbol{r}) = \delta(\frac{\sigma}{2} - r) \tag{37}$$

$$w_3(\boldsymbol{r}) = \Theta(\frac{\sigma}{2} - r) \tag{38}$$

$$w_{V1}(\boldsymbol{r}) = \frac{w_{V2}(\boldsymbol{r})}{2\pi\sigma} \tag{39}$$

and

$$w_{V2}(\boldsymbol{r}) = \frac{\boldsymbol{r}}{r}\delta(\frac{\sigma}{2} - r) \tag{40}$$

Note that the index V denotes a vector weight function. We can express this fact by writing $w_{V1} \equiv \boldsymbol{w}_{V1}$, $n_{V1} \equiv \boldsymbol{n}_{V1}$,... Finally the function Φ is given by

$$\Phi = \Phi_1 + \Phi_2 + \Phi_3 \tag{41}$$

with

$$\Phi_1 = -n_0 \ln(1 - n_3) \tag{42}$$

$$\Phi_2 = \frac{n_1 n_2 - \boldsymbol{n}_{V1} \cdot \boldsymbol{n}_{V2}}{1 - n_3} \tag{43}$$

and

$$\Phi_3 = \frac{n_3^2 (1 - (\boldsymbol{n}_{V2}/n_2)^2)^3}{24\pi(1 - n_3)^2} \tag{44}$$

Let us emphasize few points: First, the six weight functions are connected to the geometrical (fundamental) Minkowski measures. In fact, the derivation of the Rosenfeld functional requires a convolution property which can nicely be evaluated by using the linear decomposition into the four Minkowski measures for an arbitrary additive measure. One might therefore conjecture that there is a deeper connection between the geometry and density functional theory which, however, still has to be discovered and worked out! Second, Rosenfeld's functional gives the analytical Percus-Yevick direct correlation function as an output by using the relation (32). Consequently the Percus-Yevick theory is included in this density functional approach. Also the cell model is included near close-packing [77]. Hence the density functional approach provides a unifying theory of fluid and crystal. In particular, a configuration of overlapping spheres (which implies $n_3 \to 1$) is avoided as the functional gives an infinite energy penalty to such densities, see again (42) and the denominator in (43). From this respect, the Rosenfeld functional is superior to weighted density approximations proposed earlier where $c(r)$ is taken as an input and overlapping configurations of hard spheres are not excluded, for a more detailed discussion see e.g. [70]. Third, one can test the quality of any density functional by subjecting the three-dimensional functional to a strongly confining external potential such that the resulting system lives in a reduced spatial dimension. For instance, by applying a hard tube of diameter σ one can squeeze the three dimensional hard sphere system into a system of hard rods. As the density functional for hard rods is exactly known, one can test whether the resulting projected three-dimensional functional respects this dimensional crossover [78]. The ultimate reduction occurs for an external hard cavity potential that can hold only a single particle. For this trivial situation, the exact functional is known. It was shown that this limit requires some conditions which can be exploited to fix some freedom in the original functional [78]. Finally, the freezing transition can be calculated by plugging in a constant density field for the fluid phase and a lattice sum of Gaussian peaks in the solid phase. If the width of the Gaussians and the prefactor are taken as variational parameters one gets a first-order freezing transition with coexisting packing fractions of $\eta_f = 0.491$ and $\eta_s = 0.540$ which are very close to "exact" simulation data.

5 Hard Spheres and Phase Transitions: Computer Simulations

Most of our knowledge for hard sphere systems is based on "exact" results obtained by computer simulations, see e.g. [1]. In a bulk computer simulation the system is typically confined to a finite cubic box with periodic boundary conditions in all three directions to minimize finite-size effects. The typical number of particles is in the range from $N = 100$ to $N = 1000000$.

The recipe is as follows: one starts from a given overlap-free configuration of spheres. Then one generates a new configuration by using either a Molecular Dynamics code or a Monte Carlo technique. Using Molecular Dynamics means that Newton's equation of motion are solved. The hard spheres are then moving along the classical trajectories which are straight lines interrupted by elastic collisons. In Monte Carlo one randomly displaces a randomly chosen particle and checks for particle overlap: if the new configuration is free of any overlaps the move is accepted, if not it is rejected. Then one carefully has to equilibrate the system. Finally statistics is gathered to perform the canonical averages. We remark that Monte Carlo techniques are also possible in different ensembles where the pressure is fixed instead of the system volume, or the chemical potential is fixed instead of the particle number. For an example, see the method described in the contribution of Döge *et al.* in this volume.

A problem is that only averages are readily calculated by a simulation. The key quantity for phase transitions, however, is the Helmholtz free energy, which cannot be written as an average. One possible solution of this problem is to calculate the contact value $g(\sigma^+)$ of the pair distribution function which can clearly be written as an average, see (20). One thereby gains the pressure (or the reduced equation of state) by using the virial expression (22). In doing so for arbitrary densities, one can plot directly $P(\rho)$ and look for van-der-Waals loops indicating a first order phase transition, see Fig. 12. Typically the hysteresis is small decreasing with increasing system size and therefore it is difficult to see whether really a phase transition takes place. A more accurate alternative is to obtain the Helmholtz free energy F by integration as follows

$$\frac{F}{N} = k_B T[\ln(\rho_r \Lambda^3) - 1] + \int_{\rho_r}^{\rho} d\rho' \frac{P(\rho')}{\rho'^2} \tag{45}$$

Here, the reference density ρ_r is so small that the system can be considered to be an ideal gas where the free energy is known. This is the simplest way of so-called *thermodynamic integration* starting from a well-known reference system. This strategy readily applies to the fluid phase.

As a remark, the virial expression also works in the solid phase if the contact value of the spherically averaged pair distribution function is inserted into (22). However there are technical problems in applying this recipe to the solid phase as the pair distribution function strongly piles up near contact and extrapolation of $g(r)$ to contact bears a large extrapolation error. A smarter way of thermodynamic integration in the hard sphere solid is to start from an Einstein solid

[31]. Here, all particles are harmonically bound to a lattice position of a given lattice as described by an external potential H_{ext}

$$H_{ext} = \sum_{i=1}^{N} \frac{K}{2} (\boldsymbol{R}_i - \boldsymbol{R}_i^{(0)})^2 \tag{46}$$

where $\{\boldsymbol{R}_i^{(0)}\}$ are the positions of the given lattice. If the spring constant K which confines the particles to their lattice positions is very large, then the particles do not feel the hard sphere interaction. Hence the system is practically a set a decoupled harmonic oscillators for which the reference free energy F_0 can readily be calculated. Now the harmonic external potential is switched off continuously, i.e. we consider the total Hamiltonian

$$H_{tot} = H_{kin} + (1 - \lambda) H_{ext} + V_{int} \tag{47}$$

where H_{kin} is the total kinetic energy, V_{int} is the pairwise hard core interaction, and the parameter λ is a formal coupling parameter by which we can switch off continuously the external harmonic potential and turn on the hard-core interaction.. It is readily calculated that the derivative $\partial F/\partial\lambda|_{T,\Omega,N}$ can be written as an average:

$$\begin{aligned} \frac{\partial F}{\partial \lambda} &= -k_B T \frac{\frac{\partial Z}{\partial \lambda}}{Z} = - < H_{ext} >_\lambda \\ &= -\frac{NK}{2} < (\boldsymbol{R}_i - \boldsymbol{R}_i^{(0)})^2 >_\lambda \end{aligned} \tag{48}$$

Here the canonical average $< ... >_\lambda$ means that an external potential of strength $1 - \lambda$ is present. (48) implies that one has to calculate the Lindemann parameter (or the mean-square-displacement) of the solid in order to access $\partial F/\partial\lambda$. Finally integration with respect to λ yields the desired free energy:

$$F = F_0 + \int_0^1 d\lambda \frac{\partial F}{\partial \lambda} \tag{49}$$

It is important to remark that one needs a whole set of simulations (for different λ) to access a single free energy. In practice typically 10-30 integration points are needed to get a good accuracy. Apart from numerical integration errors and statistical and finite-system-size errors, this methods leads in principle to exact results for the free energy. The only requirement is that one should not cross a phase boundary during the integration. Also the lattice structure is not known a priori but different lattice types have to be tried and the resulting free energy which is minimal corresponds to the realized structure.

Computer simulations of the hard sphere system have given a coherent picture of what is going on as far as phase transformations of the system are concerned. By a careful study of finite system size effects it has been established from the early days of computer simulation [45] that the hard sphere system freezes indeed from a fluid into an ordered solid with a strongly first-order transition, i.e. the density jump across the transition is pretty large. The data of the

coexisting packing fractions are $\eta_f = 0.494$ and $\eta_s = 0.545$. The phase diagram is sketched in Fig. 13. The combination of Percus-Yevick and cell theory gives coexistence densities that are too high while there is perfect agreement with density functional theory.

There is another interesting non-equilibrium phase transition for $\eta = \eta_G \approx 0.58$ where a rapidly compressed hard sphere fluid freezes into an amorphous glass as signalled by a very slow decay of dynamical correlations. However, if one waits for a long time, the system will recrystallize in its thermodynamically stable solid [27]. Above a certain threshold density $\eta_{RCP} \approx 0.64$ called random-closed packing there is no glass transition possible and the system is forced to freeze into a regular solid. We finally mention that the whole phase diagram including the glass transition was confirmed in detail by experiments on sterically-stabilized colloidal suspensions [75].

What is the stable crystal lattice away from close-packing? This question has attracted some attention in the past years. A simple cubic and body-centered-cubic lattice can be ruled out from the very beginning, since these lattices are mechanically unstable with respect to shear. A tricky competition arises between the possible close-packed structures fcc, hcp, double hcp, and random stacking, see again chapter 1. It was shown by computer simulation [14,17,58,74] that for $\eta_s < \eta < \eta_{cp}$ an fcc solid has a slightly lower free energy than all other stacking sequences, but the relative difference in the free energy per particle is smaller than $10^{-3} k_B T$.

As already mentioned in chapter 2, the freezing transition in the hard disk system is much more difficult to compute by simulation and is still controversial. The reason is that the transition is not strongly first order as for the hard sphere system. Therefore the free energy differences are tiny and also finite system size effects are much more pronounced in two spatial dimensions.

6 A Selection of Recent Research Activities on Hard-Sphere-Like Systems

6.1 Binary Mixtures

It is straightforward to generalize the one-component hard-sphere model to two species. The three parameters determining the system are now the diameter ratio $q = \sigma_1/\sigma_2 \leq 1$ and the two partial packing fractions, η_s and η_l of the small and big spheres. Obviously, the one-component model is obtained as the special case $q = 1$.

Depending on the ratio q, one might expect quite different phase diagrams. If q is not much different from 1, then an fcc crystal is stable which is randomly occupied by the two species. Computer simulations [52] and numerous density functional calculations (see e.g.[22,23] have been performed here. The results for the phase diagram are in accordance with measurements on sterically-stabilized colloidal suspensions.

For intermediate q, there are more exotic crystalline phases. For certain values of q there are crystalline solids with an AB AB_2 and AB_{13} (superlattice) structure. These structures were obtained by experiments [4], computer simulation [28], density functional [90] and cell theory [5] studies and demonstrate nicely the fruitful interaction between these different approaches. The existence of such solid lattices crucially depends on the close-packed structure. Even more complicated lattice structures can be expected upon further reducing q. Also it has been speculated about the existence of stable quasicrystals for certain ratios q although they can most probably be ruled out for $q > 0.85$ [59]. The stability of quasicrystals is closely related to the question whether the close-packed structure is a periodic lattice or not. There is no mathematical proof known for general q.

Another interesting case is the limit of small q. Here there has been some debate about possible phase separation over the last decade. An analytical Percus-Yevick solution is possible predicting no fluid-fluid phase separation for hard sphere mixtures but the theory fails in the limit of $q \to 0$ if η_s and η_l is kept finite [10]. The phase diagram of strongly asymmetric hard sphere mixtures was recently obtained by computer simulations by Dijkstra, van Roij and Evans [25,26] which answered the story after all. For three different ratios $q = 0.2, 0.1, 0.05$ the phase diagrams are shown in Fig. 14. In fact a fluid-fluid phase separation is preempted by the fluid-solid transition but an isostructural solid-solid transition shows up for high packing fractions of the large particle due to the strong and short-ranged depletion attraction induced by the small particles [38].

Finally we remark that the kinetic glass transition is different for large and for small q. While both particle species freeze-in simultaneously for $q \approx 1$, there is a crossover at $q_c \approx 0.15$ where the big spheres are frozen-in on a lattice and the small spheres are still liquid-like. This was found theoretically [16,64,65] and confirmed experimentally for colloidal suspensions [46,47].

6.2 Size Polydispersity

A size-polydisperse hard-sphere system can be understood as a mixture with an infinite number of different species whose diameter is distributed according to a normalized probability function $p(\sigma)$. A relative small distribution is characterized by its first two moments, or equivalently by its mean diameter $\bar{\sigma} = \int d\sigma p(\sigma)$ and the relative polydispersity $s^2 = \bar{\sigma^2}/\bar{\sigma}^2 - 1$. A study of effects induced by polydispersity is important if one has a quantitative comparison with a real colloidal sample in mind. It has been established by density functional theory [3] and computer simulation [12,13,51] that above a certain critical polydispersity of roughly 6% a solid lattice is no longer stable. The corresponding phase diagram is shown in Fig. 15. A regular random occupied solid lattice structure coexists with a fluid that has a higher polydispersity as the solid as indicated by the tie-lines in Fig. 15. For high densities the solid exhibits reentrant melting into an amorphous phase [7].

At higher polydispersities, the phase behaviour depends more and more on the details of the diameter distribution $p(\sigma)$. A randomly occupied solid is expected to separate into two or more solids with different lattice constants [5,82]. Also fluid-fluid phase separations are probable to occur 21,87]. We finally mention that the Percus-Yevick direct correelation fucntion can be explicitly calculated involving only the first three moments of the diameter distribution [11] and that the cell model is again a reliable description of the solid for high densities and small polydispersities [72].

6.3 Hard Spheres near Hard Plates

A planar hard wall can be described as an external potential

$$V_{ext}(z) = \begin{cases} \infty \text{ if } z < \sigma/2 \\ 0 \quad \text{else} \end{cases} \tag{50}$$

where z is the coordiante perpendicular to the wall. The insertion of such a planar hard plate costs free energy as there are less configurations possible. This additional free energy scales with the plate surface and gives rise to a positive surface free energy γ. For a fluid phase in contact with a wall, scaled particle theory makes a theoretical prediction for γ. In Fig. 16, γ is plotted versus the bulk packing fraction η. The agreement between scaled particle theory, density functional theory [37] and computer simulation [42,43] is convincing. If a solid is in contact with a hard wall, γ depends on the orientation. It has recently be shown that the cell model provides a reasonable analytical theory for γ which agrees perfectly with the computer simulation data [43].

For a fluid in contact with a hard wall, there is an interesting wetting effect if the bulk density is slightly below bulk freezing. Precrystallization on the hard walls [20] occurs, i.e. few layers on top of the wall have an in-plane long-ranged order corresponding to a intersecting triangular lattice sheets.

Other interesting phase transitions occur for two parallel hard plates with a slit distance H. The phase diagram depends solely on two parameters, namely the

reduced density $\rho_H = N\sigma^3/(AH)$ (where A is the system area) and the reduced plate distance $h = H/\sigma - 1$. Clearly one can continuously interpolate between two and three spatial dimensions by tuning the plate distance: For $H = \sigma$, our model reduces to that of two-dimensional hard discs while for $H \to \infty$ the three-dimensional bulk case is recovered.

The equilibrium phase diagram as obtained by Monte-Carlo computer simulation in the $\rho_H - h$-plane [80,81] is shown in Fig. 17 for moderate plate distances h. The phase behaviour is very rich and much more complicated than in the bulk. Cascades of different solid-solid transitions are found. For low densities the stable phase is an inhomogeneous fluid. All possible stable solid phases are also realized as close-packed configurations [71,73] for a certain plate distance. Accordingly one finds stable layered structures involving intersecting triangular lattices ($1\triangle$, $2\triangle$) and intersecting square lattices ($2\square$). Also a buckled phase (b) and a phase with a rhombic elementary cell (rhombic phase (r)) are stable. All transitions are first-order. Results of the cell model together with a simple fluid state theory are given in Fig. 18. Clearly the simple cell theory gives the correct topology of the phase diagram.

Similar phases were found in experiments of highly salted charged colloids between glass plates [62,63,68,86,88]. Here even higher reduced plate distances were studied. There is compelling evidence that a prism-phase consisting of alternating prisms built up by spheres is the close-packed configuration in certain domains of h [68]. Still a full quantitative mapping of the experimental data onto the theoretical phase digram of Fig. 17 has to be performed.

Let us comment on further related aspects: First it would be nice to perform a full theoretical calculation for the phase diagram of hard spheres between hard plates using a density functional calculation with Rosenfeld's functional. Second, one should investigate different confining shapes. Intriguing examples are circular and polyhedral boundaries in two dimensions. Studies have been made for confined hard discs [66] and confined hard spheres within spherical cavities [67]. Finally it is an unsolved mathematical problem to rigorously establish the close-packed structure for different h.

6.4 Hard Spherocylinders

Finally let us discuss phase transitions for hard convex bodies that are non-spherical, for a recent review see [2]. In particular, if these bodies are rotational invariant around one axis they may serve as a model for colloidal liquid crystals [54]. In particular hard spherocylinders with an additional orientational degree of fredom have been studied. These are spherical capped cylinders of cylindrical length L and diameter σ whose anisotropy is characterized by the aspect ratio $p = L/\sigma$. For $p = 0$ one recovered the case of hard spheres. The phase diagram of hard spherocylinders depends on the aspect ratio p as well as on the particle density ρ. It has recently been explored by computer simulations [14] and is shown in Fig. 19. A number of mesophases or liquid-crystalline phase are stable in the plane spanned by p and ρ. There is a plastic (or rotator) crystals for small p. For larger p, a nematic and a smectic A phase become stable for

intermediate densities. Possible stacking sequences in the solid phase are AAA where all triangular sheets are put directly on top of each other and ABC which is the close-packed structure. Note that the AAA stacking sequence is not a close-packed situation but is still stable for intermediate densities. Cell theory combined with scaled particle theory can reproduce this diagram satisfactorily [39]. Also density functional theory studies have been performed [40,44]. However, it is not easy to generalize Rosenfeld's theory to the case of anisotropic particles.

7 Conclusions

To summarize: Systems of hard spheres and its variants show interesting phase transitions. Although they are purely entropically driven, they exhibit ordering transitions. These transitions are seen in theory, computer simulation and in real matter, namely in sterically-stabilized colloidal suspensions.

A few final remarks are in order: First, there are further fascinating phenomena occurring for dynamial correlations and non-equilibrium situations of hard sphere systems [36] which have not been addressed at all in this article. Another field of physics where hard sphere system play an important role are simulations of granular matter [56]. Second, most stable crystalline phases observed in phase diagrams of hard sphere problems are close-packed ones. Therefore it would be very helpful to provide mathematical proofs for the close-packed structures in confining geometry.

As a final perspective, such simple intuitive systems as hard spheres are nontrivial enough to be studied also over the next decades. One might surmise that further interesting unexpected transitions will be discovered in the near future. Hence the final conclusion is that hard spheres are fun both for physicists and for mathematicians.

Acknowledgments:
I thank Matthias Schmidt, Martin Watzlawek, Arben Jusufi, Martin Heni, Yasha Rosenfeld, Thomas Palberg, Reimar Finken, and Siegfried Dietrich for helpful remarks. I am grateful to D. Stoyan, Joachim Dzubiella, and Matthias Schmidt for a critical reading of the manuscript. Financial support by the Deutsche Forschungsgemeinschaft via the Schwerpunktsprogramm Benetzung und Strukturbildung an Grenzflächen is gratefully acknowledged.

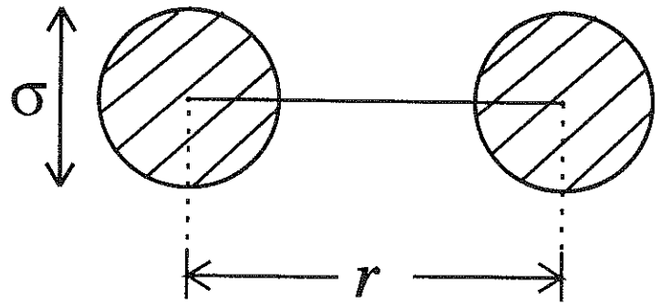

Fig. 1. Two hard spheres of diameter σ at center-of-mass distance r.

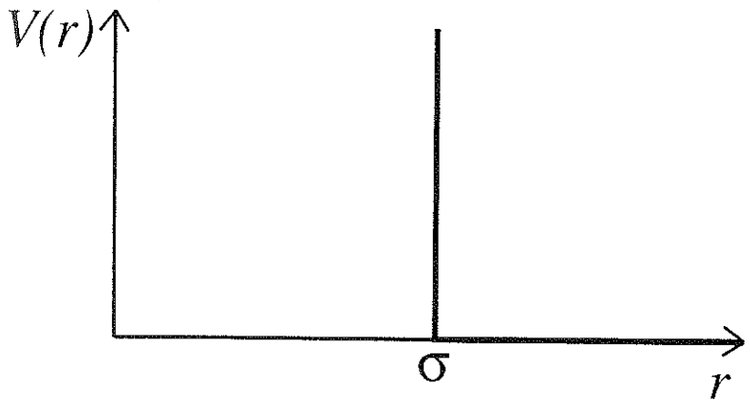

Fig. 2. Pair potential of hard spheres $V(r)$ as a function of their center-of-mass distance r.

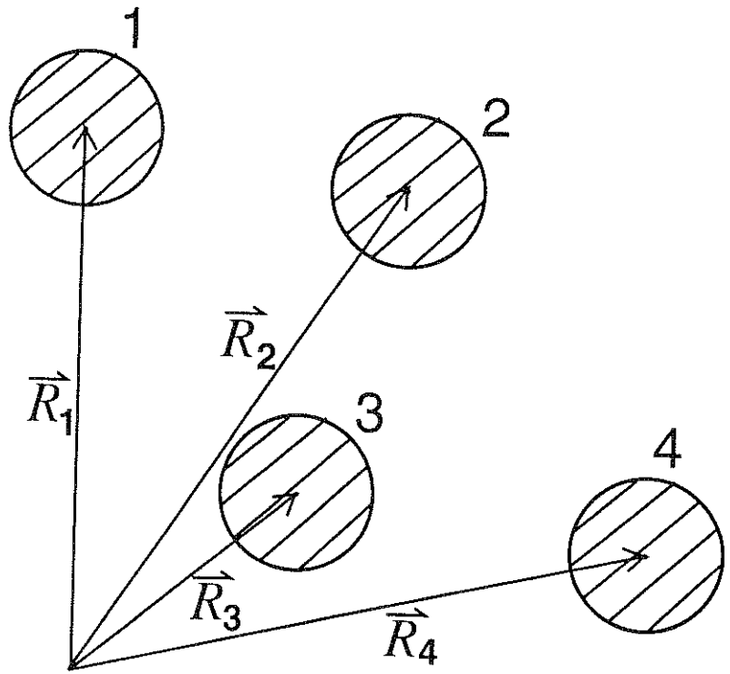

Fig. 3. Configuration $\{\boldsymbol{R}_i\}$ $(i = 1, 2, 3, 4)$ of four hard spheres.

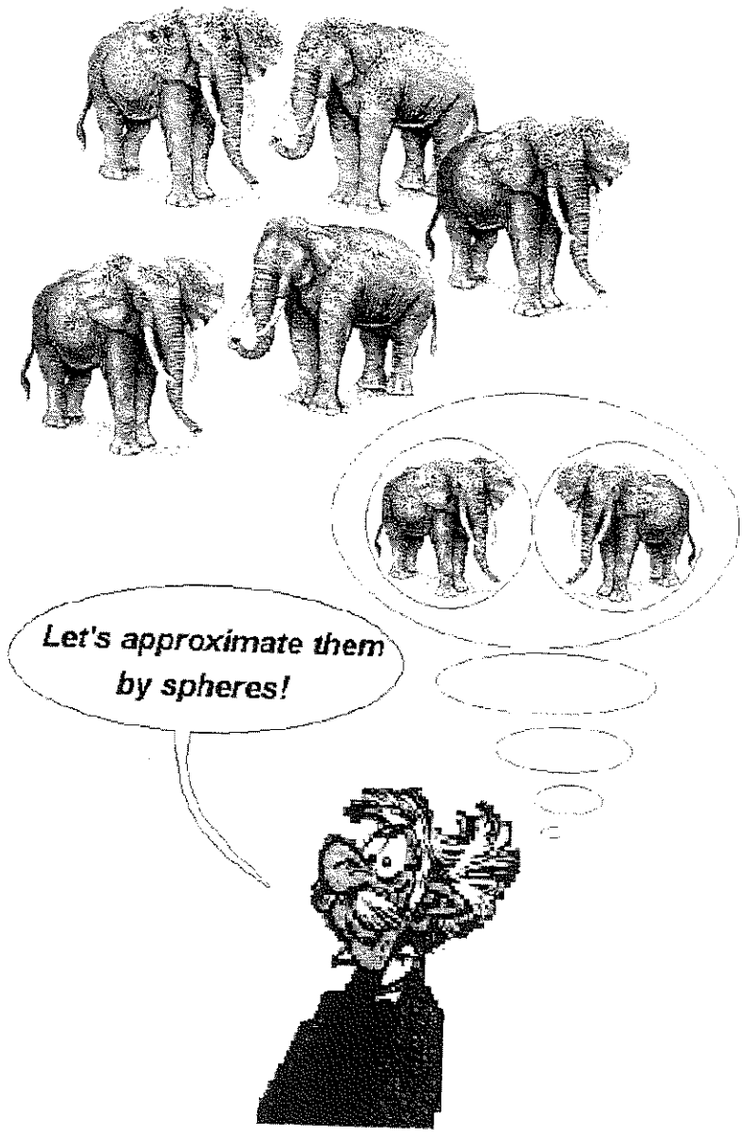

Fig. 4. The hard sphere model at work: zeroth approximation for almost any problem in the brain of the theoretician.

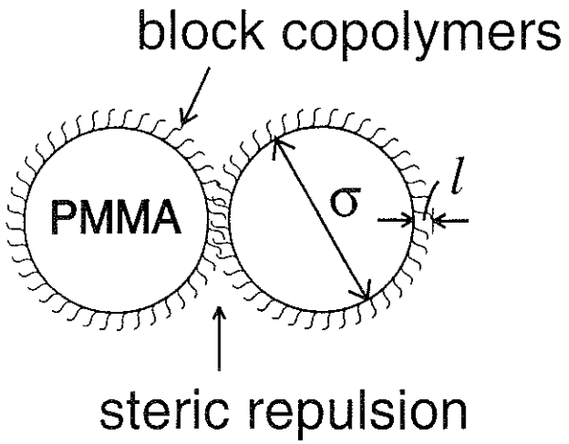

Fig. 5. Sterically-stabilized colloidal suspensions of PMMA spheres with coated block copolymer brushes of length ℓ.

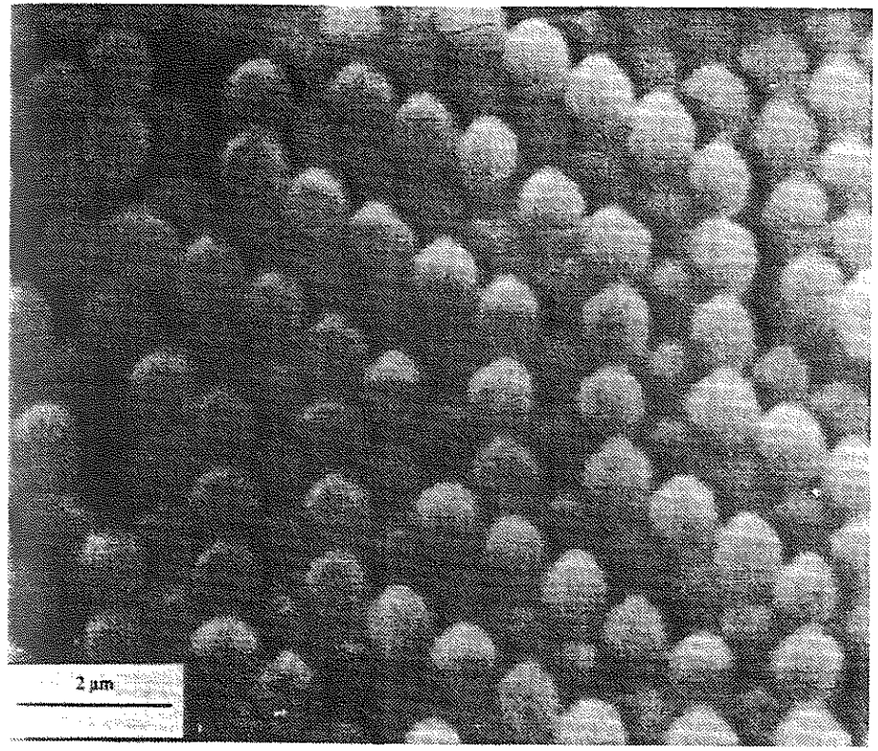

Fig. 6. Electron micrograph of colloidal microspheres. From [69].

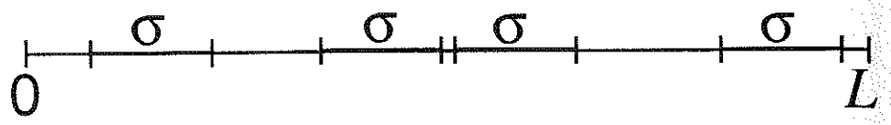

Fig. 7. Hard sphere model in one spatial dimensions: hard rods along a line of length L.

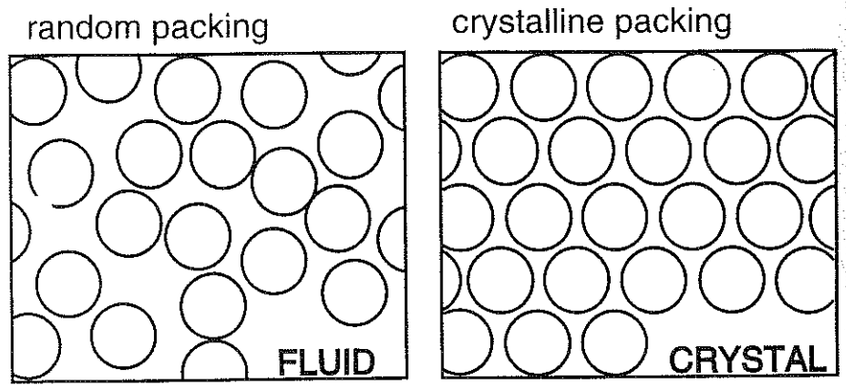

Fig. 8. Random configuration in the fluid phase and regular packed configuration in the solid phase of a hard disk system.

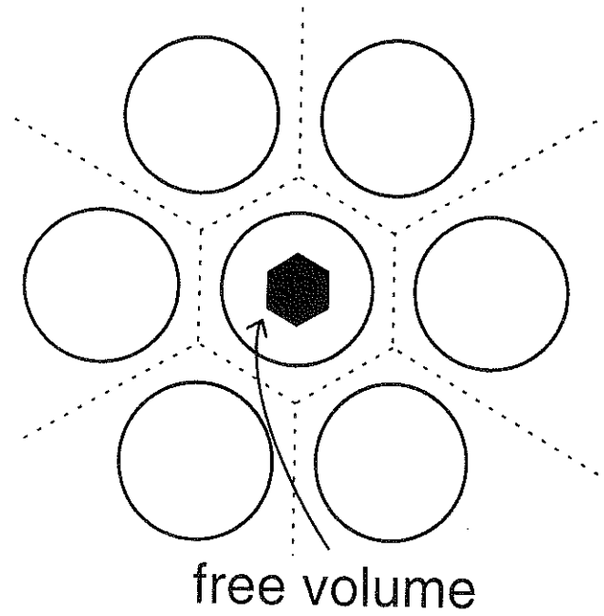

Fig. 9. Cell theory for the hard sphere crystal. The Wigner-Seitz cell (dashed line) and the free-volume cell is shown schematically.

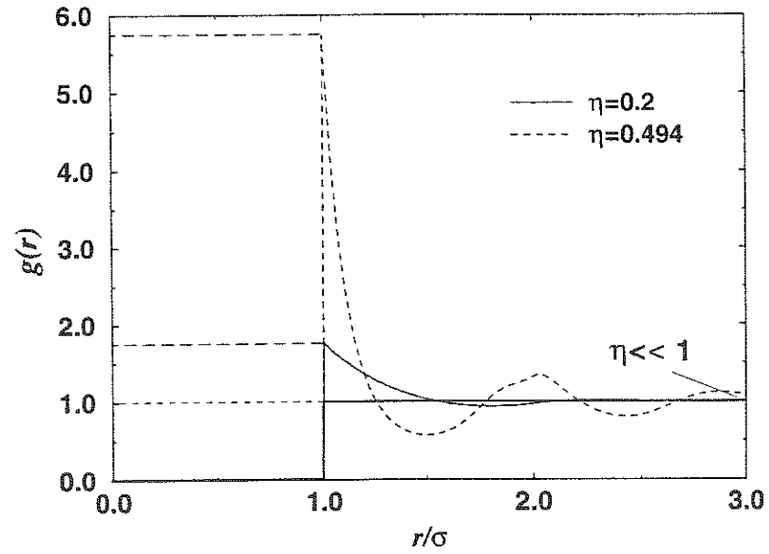

Fig. 10. Pair distribution function $g(r)$ for hard spheres as a function of distance r for small densities (dashed step function), for $\eta = 0.2$ (dotted line) and for $\eta = 0.494$ (solid line).

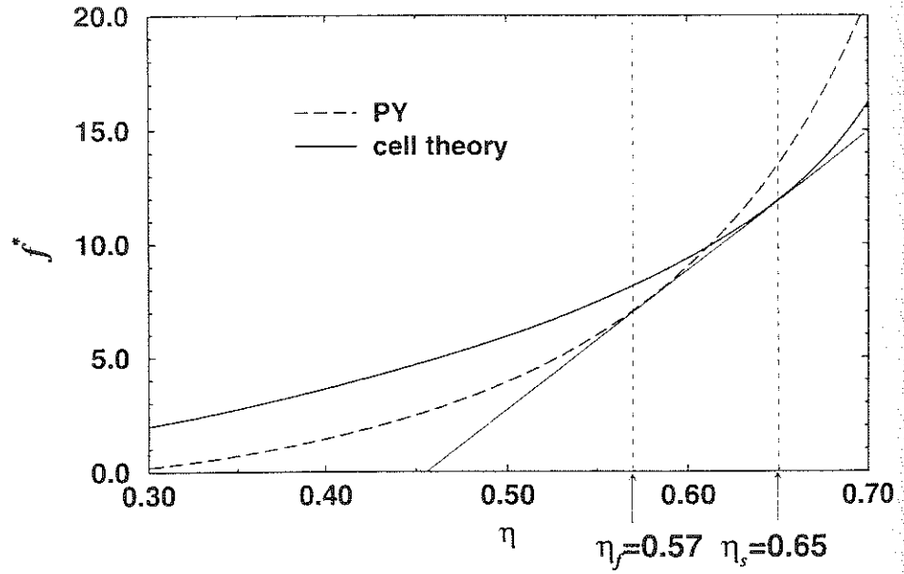

Fig. 11. Reduced free energy per unit volume $f^* = f\sigma^3/k_BT$ versus packing fraction η. The dashed line is the Percus-Yevick virial expression, the solid line is from solid cell theory. The Maxwell common tangent is also shown.

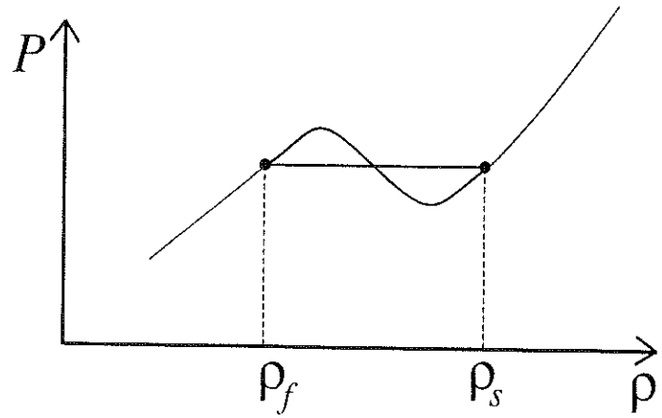

Fig. 12. Isothermal equation of state P as a function of density. The Maxwell equal-area construction is shown.

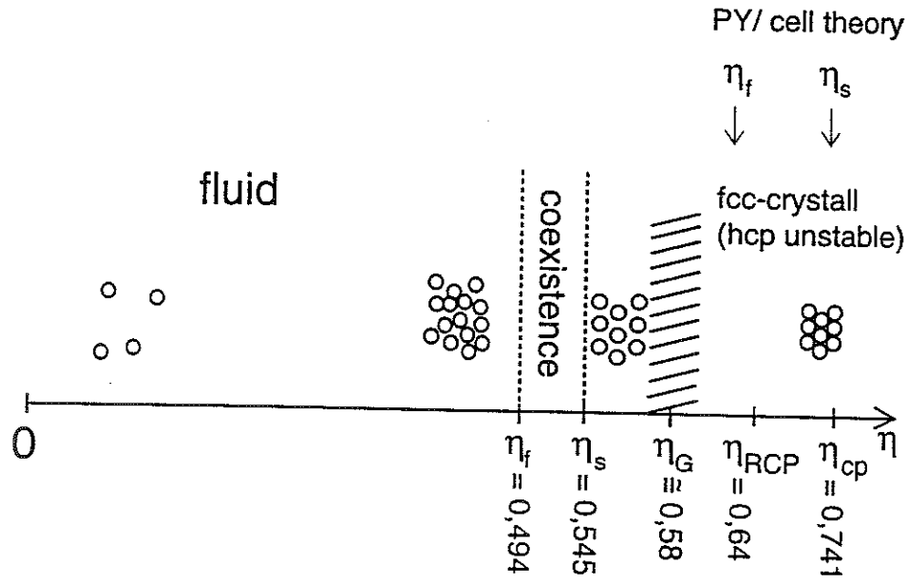

Fig. 13. Phase diagram of hard spheres versus packing fraction η. The freezing transition together with the two coexisting packing fractions η_f and η_s are shown. Also the glass transition is indicated.

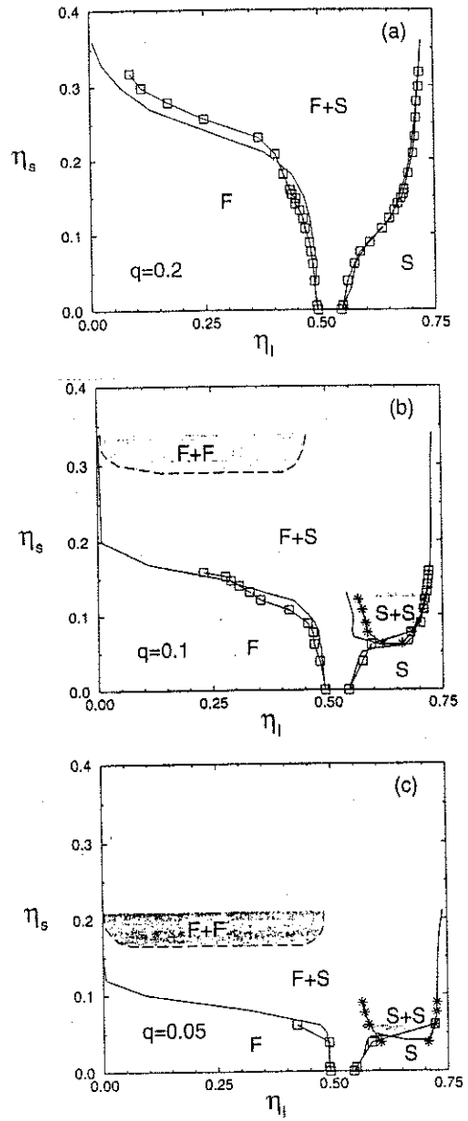

Fig. 14. Phase diagram of a binary hard-sphere mixtures with size ratio (a) $q = 0.2$, (b) $q = 0.1$, (c) $q = 0.05$ as a function of the large sphere packing fraction η_l and the small sphere packing fraction η_s. F and S denote the stable fluid and solid (fcc) phase. $F + S$, $F + F$, and $S + S$ denote, respectively, the stable fluid-solid, the metastable fluid-fluid and (meta) stable solid-solid coexistence region. The solid and dashed lines are from one effective one-component depletion potential. The symbols joined by lines to guide the eye are from computer simulations of the full binary system. From [26].

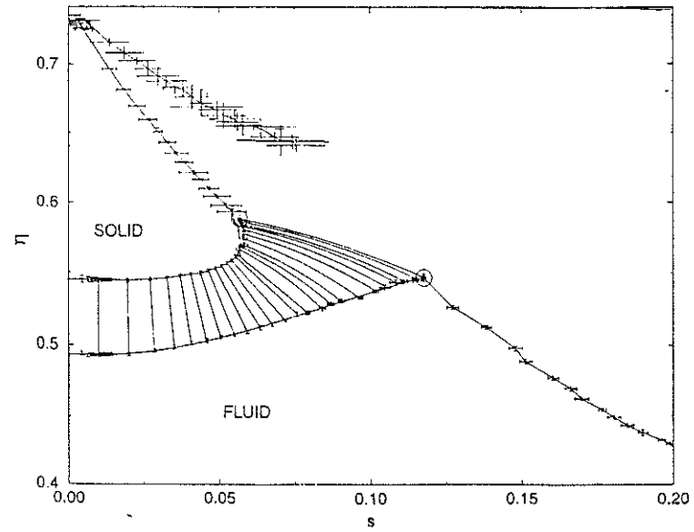

Fig. 15. Phase diagram of polydisperse hard spheres in the η, s plane. The fluid and solid phase together with their tie-lines are shown. The terminating polydispersity for a solid phase is roughly 6%. From [12,13].

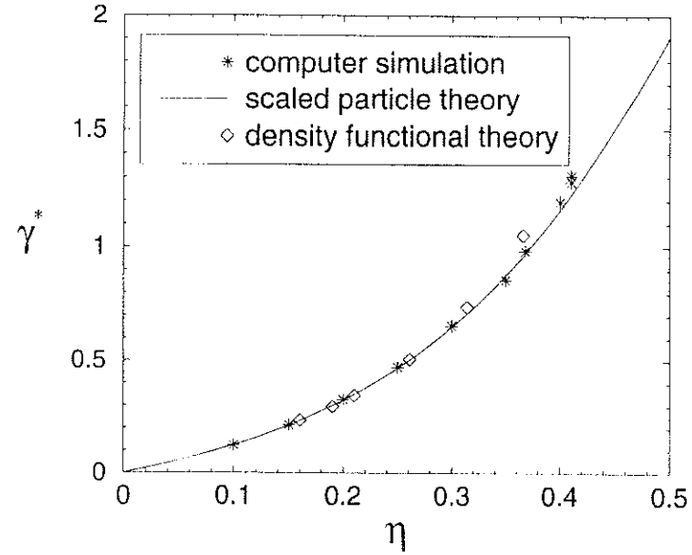

Fig. 16. Reduced interfacial free energy $\gamma^* = \gamma\sigma^2/k_BT$ of the hard sphere fluid in contact with a hard wall versus bulk packing fraction η. Solid line: scaled-particle theory; $*$: simulation data from [42] and [43]; diamonds: density functional results from [37].

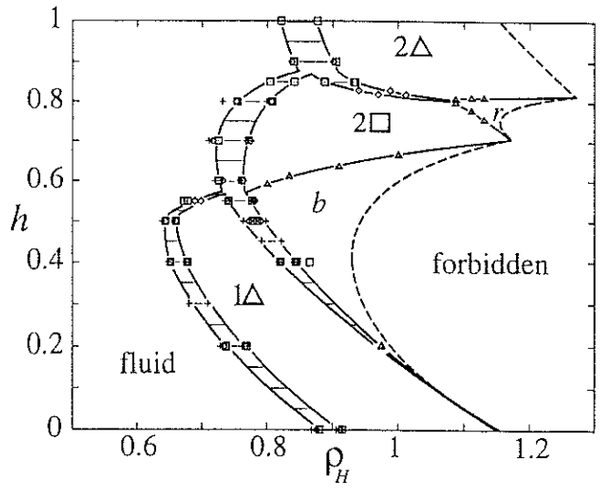

Fig. 17. Phase diagram for hard spheres of reduced density ρ_H between parallel plates with effective reduced distance h. Symbols indicate different system sizes: $N = 192(+); N = 384, 512(\diamond); N = 576(\triangle); N = 1024, 1156(\square)$. Six phases occur (fluid, $1\triangle$, b, $2\square$, r and $2\triangle$) . The closed-packed density is marked by a dashed line. Solid lines are guides to the eye. Thin horizontal lines represent two-phase coexistence. From [80].

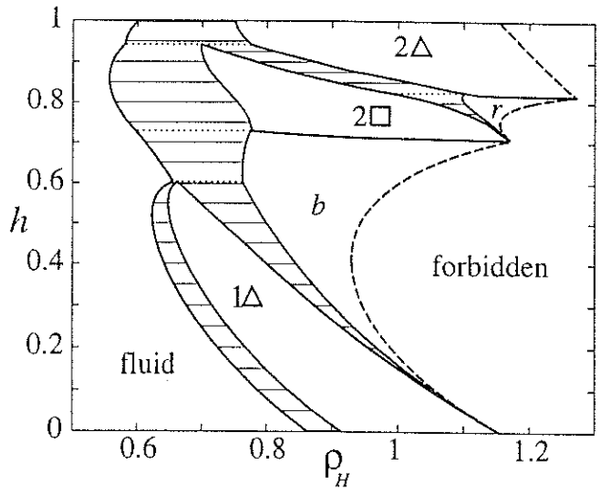

Fig. 18. Same as Fig. 17, but now obtained within the cell model for the solid phases and a simple mapping theory for the fluid phase. From [81].

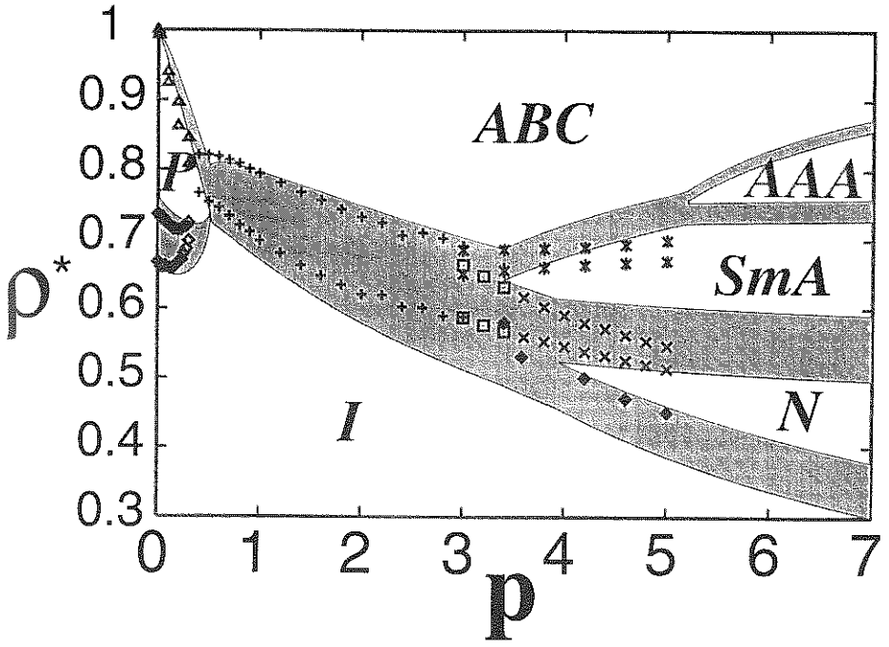

Fig. 19. Phase diagram of hard spherocylinders obtained by cell and scaled-particle theory in the $\rho^* - p$ plane where $\rho^* \equiv \eta/\eta_{cp}$. The coexistence regions are shown as shaded areas. Simulation results from [15] are shown as dots. There is an isotropic fluid (I), an ABC-stacked solid, an AAA stacked solid, a plastic crystal (P), a nematic (N) and a smectic-A (SmA) phase. The meaning of the symbols for the simulational data are: (+) I-ABC transition, ($\diamond$) I-P transition, ($\square$) I-SmA transition, ($\blacklozenge$) I-N transition, ($\times$) N-SmA transition, ($*$) SmA-ABC transition, ($\blacktriangle$) P-ABC transition. From [39].

References

1. Allen, M.P., D.J. Tildesley (1989): *Computer Simulation of Liquids* (Clarendon Press, Oxford)
2. Allen, M.P., G.T. Evans, D. Frenkel, B. M. Mulder (1993): 'Hard Convex Body Fluids', *Advances in Chemical Physics*, Vol. **LXXXVI**, pp. 1–166
3. Barrat, J.L., J.P. Hansen (1986): 'On the stability of polydispersed colloidal crystals', *J. Physique* **47**, Paris, pp. 1547–1553
4. Bartlett, P., R.H. Ottewill, P.N. Pusey (1992): 'Superlattice Formation in Binary Mixtures of Hard-Sphere Colloids', *Phys. Rev. Letters* **68**, pp. 3801–3804
5. Bartlett, P. (1997): 'A geometrically-based mean-field theory of polydisperse hard-sphere mixture', *J. Chem. Phys.* **107**, pp. 188–196

6. Bartlett, P. (1998): 'Fractionated crystallization in a polydisperse mixture of hard spheres', *J. Chem. Phys.* **109**, pp. 10970–10975
7. Bartlett, P., P.B. Warren (1999): 'Reentrant Melting in Polydispersed Hard Spheres', *Phys. Rev. Letters* **82**, pp. 1979–1982
8. Barker, J.A., D. Henderson (1976): 'What is a "liquid"? Understanding the states of matter', *Rev. Mod. Phys.* **48**, pp. 587–676
9. Baus, M. (1987): 'Statistical Mechanical Theories of Freezing: An Overview', *J. Stat. Phys.* **48**, pp. 1129–1146
10. Biben T., J.P. Hansen (1991): 'Phase Seperation of Asymmetric Binary Hard-Sphere Fluids', *Phys. Rev. Letters* **66**, pp. 2215–2218
11. Blum, L. and G. Stell (1979): 'Polydisperse systems. I. Scattering function for polydisperse fluids of hard or permeable spheres', *J. Chem. Phys.* **71**, pp. 42–46
12. Bolhuis, P.G., D.A. Kofke (1996a): 'Numerical study of freezing in polydisperse colloidal suspensions', *J. Phys. Condensed Matter* **8**, pp. 9627–9631
13. Bolhuis, P.G., D.A. Kofke (1996b): 'Monte Carlo study of freezing of polydispersed hard spheres', *Phys. Rev. E* **54**, pp. 634–643
14. Bolhuis, P.G., D. Frenkel, S.-C. Mau, D.A. Huse (1997): 'Fatigue, alcohol and performance impairment', *Nature* **388**, London, pp. 235–238
15. Bolhuis, P.G., D. Frenkel (1997): 'Tracing the phase boundaries of hard spherocylinders', *J. Chem. Phys.* **106**, pp. 666–687
16. Bosse, J., J.S. Thakur (1987): 'Delocalization of Small Particles in a Glassy Matrix', *Phys. Rev. Letters* **59**, pp. 998–1001
17. Bruce, A.D., N.B. Wilding, G.J. Auckland: 'Free Energy of Crystalline Solids: A Lattice-Switch Monte Carlo Method', *Phys. Rev. Letters* **79**, pp. 3002–3005
18. Callen, H.B. (1960): *Thermodynamics* (Wiley, New York)
19. Cipra, B. (1998): 'Packing Challenge Mastered At Last', *Science* **281**, p. 1267
20. Courtemanche, D.J., F. van Swol (1992): 'Wetting State of a Crystal Fluid System of Hard Spheres', *Phys. Rev. Letters* **69**, pp. 2078–2081
21. Cuesta, J.A. (1999): 'Demixing in a single-peak distributed polydisperse mixture of hard spheres', *Europhysics Letters* **46**, pp. 197–203
22. Denton, A.R., N.W. Ashcroft (1990): 'Weighted-density-functional theory of nonuniform fluid mixtures: Application to freezing of binary hard-sphere mixtures', *Phys. Rev. A* **42**, pp. 7312–7329
23. Denton, A.R., N.W. Ashcroft (1991): 'Vegard's law', *Phys. Rev. A* **43**, pp. 3161–3164
24. Dietrich, S. (1988):'Wetting Phenomena'. In: *Phase transitions and Critical Phenomena*, ed. by C. Domb, J.L. Lebowitz, Vol. 12 (Academic Press, London), pp. 1–128
25. Dijkstra, M., R. van Roij, R. Evans (1999a): 'Direct Simulation of the Phase Behaviour of Binary Hard-Sphere Mixtures: Test of the Depletion Potential Description', *Phys. Rev. Letters* **82**, pp. 117–120
26. Dijkstra, M., R. van Roij, R. Evans (1999b): 'Phase diagramm of highly asymmetric binary hard-sphere mixtures', *Phys. Rev. E* **59**, pp. 5744–5771
27. Doliwa, B., A. Heuer (1998): 'Cage Effect, Local Anisotropies and Dynamic Heterogeneities at the Glass Transiton: A Computer Study of Hard Spheres', *Phys. Rev. Letters* **80**, pp. 4915–4918
28. Eldridge, M.D., P.A. Madden, D. Frenkel (1993): 'The stability of the AB_{13} crystal in a binary hard sphere system', *Mol. Phys.* **79**, pp. 105–120
29. Evans, R. (1992): 'Density Functionals in the Theory of Nonuniform Fluids'. In: *Fundamentals of Inhomogeneous Fluids*, ed. by D. Henderson (Marcel Dekker, New York), pp. 85–176

30. Finken, R., M. Schmidt, H. Löwen: to be published
31. Frenkel, D., B. Smit (1996): *Understanding Molecular Simulation* (Academic, San Diego)
32. Frisch, H.L., N. Rivier and D. Wyler (1985): 'Classical Hard-Sphere Fluid in Infinitely Many Dimensions', *Phys. Rev. Letters* **54**, pp. 2061–2063
33. Frisch, H.L., J.K. Percus (1987): 'Nonuniform classical fluid at high dimensionality', *Phys. Rev. A* **35**, pp. 4696–4702
34. Frisch, H.L., J.K. Percus (1999): 'High dimensionality as an organizing device for classical fluids', *Phys. Rev. E* **60**, pp. 2942–2948
35. Fröhlich, J., C. Pfister (1981): 'On the Absence of Spontaneous Symmetry Breaking and of Crystalline Ordering in Two-Dimensional Systems', *Commun. Math. Phys.* **81**, pp. 277–298
36. Garzo, V., J.W. Dufty (1999): 'Dense fluid transport for inelastic hard spheres', *Phys. Rev. E* **59**, pp. 5895–5911
37. Götzelmann, B., A. Haase, S. Dietrich (1996): Structure factor of hard spheres near a wall', *Phys. Rev. E* **53**, pp. 3456–3467
38. Götzelmann, B., R. Evans, S. Dietrich (1998): 'Depletion forces in fluids', *Phys. Rev. E* **57**, pp. 6785–6800
39. Graf, H., H. Löwen, M. Schmidt (1997): 'Cell theory for the phase diagram of hard spherocylinders', *Prog. Colloid Polymer Science* **104**, pp. 177–179
40. Graf, H., H. Löwen (1999): 'Density functional theory for hard spherocylinders: phase transitions in the bulk in the presence of external fields', *J. Phys. Condensed Matter* **11**, pp. 1435–1452
41. Hansen, J.P., I.R. McDonald (1986): *Theory of Simple Liquids*, 2nd ed. (Academic Press, London)
42. Henderson, J.R., F. van Swol (1984): 'On the interface between fluid and a planar wall: Theory and simulations of a hard sphere fluid at a hard wall', *Mol. Phys.* **51**, pp. 991-1010
43. Heni, M., H. Löwen (1999): 'Interfacial free energy of hard sphere fluids and solids near a hard wall', *Phys. Rev. E* (in press)
44. Holyst, R., A. Poniewierski (1989): 'Nematic-smectic-A transition for perfectly aligned hard spherocylinders: Application of the smoothed-density approximation', *Phys. Rev. A* **39**, pp. 2742–2744
45. Hoover, W.G., F.H. Ree (1968): 'Melting Transitions and Communal Entropy for Hard Spheres', *J. Chem. Phys.* **49**, pp. 3609–3617
46. Imhof, A., J.K.G. Dhont (1995): 'Long-time self-Diffusion in binary colloidal hard-sphere dispersions', *Phys. Rev. E* **52**, pp. 6344–6357
47. Imhof, A., J.K.G. Dhont (1997): 'Phase behaviour and long-time self-diffusion in a binary hard sphere dispersion', *Colloids and Surfaces* **122**, pp. 53–61
48. Jaster, A. (1998): 'Orientational order of the two-dimensional hard-disk system', *Europhys. Letters* **42**, pp. 277–282
49. Jaster, A. (1999): 'Computer simulations of the two-dimensional melting transition using hard disks', *Phys. Rev. E* **59**, pp. 2594–2602
50. Kirkpatrick, T.R. (1986): 'Ordering in the parallel hard hypercube gas', *J. Chem. Phys.* **85**, pp. 3515–3519
51. Kofke, D.A., P.G. Bolhuis (1999): 'Freezing of polydisperse hard spheres', *Phys. Rev. E* **59**, pp. 618–622
52. Kranendonk, W.G.T., D. Frenkel (1991): 'Thermodynamic properties of binary hard sphere mixtures', *Mol. Phys.* **72**, pp. 715–733
53. Lebowitz, J.L., O. Penrose (1964): 'Convergence of virial expansions', *J. Math. Phys.* **5**, pp. 841–847

54. Lekkerkerker, H.N.W., P. Buining, J. Buitenhuis, G.J. Vroege, A. Stroobants (1995): 'Liquid Crystal Phase Transition in Dispersions of Rodlike Colloidal Particles'. In: *Observation, Prediction and Simulation of Phase Transitions in Complex Fluids*, ed. by M. Baus et al. (Kluwer, Holland), pp. 53–112
55. Leppmeier, M. (1997): *Kugelpackungen: von Kepler bis heute* (Vieweg, Wiesbaden)
56. Luding, S. (1995): 'Granular materials under vibration: simulations of rotating spheres', *Phys. Rev. E* **52**, pp. 4442–4457
57. Löwen, H. (1994): 'Melting, Freezing and Colloidal Suspensions', *Phys. Rep.* **237**, pp. 249–324
58. Mau, S.-C., D.A. Huse (1999): 'Stacking entropy of hard-sphere crystals', *Phys. Rev. E* **59**, pp. 4396–4401
59. McCarley, J.S., N.W. Ashcroft (1994): 'Hard-Sphere quasicrystals', *Phys. Rev. B* **49**, pp. 15600–15606
60. Mitus A.C., H. Weber, D. Marx (1997): 'Local structure analysis of the hard-disk fluid near melting', *Phys. Rev. E* **55**, pp. 6855–6857
61. Münster, A. (1974): *Statistical Thermodynamics*. Vol. **II** (Springer-Verlag, Berlin), pp. 337–346
62. Murray, C.A., W.O. Sprenger, R.A. Wenk (1990): 'Comparison of melting in three and two dimensions: Microscopy of colloidal spheres', *Phys. Rev. B* **42**, pp. 688–703
63. Murray, C.A. (1992): 'Experimental Studies of Melting and Hexatic Order in Two-Dimensional Colloidal Suspensions'. In: *Bond-orientational Order in Condensed Matter Systems*, ed. by K.J. Strandburg (Springer, New York), pp. 137–215
64. Nägele, G., J.K.G. Dhont (1998): 'Tracer-diffusion in colloidal mixtures: A mode-coupling scheme with hydrodynamic interactions', *J. Chem. Phys.* **108**, pp. 9566–9576
65. Nägele, G., J. Bergenholtz (1998): 'Linear viscoelasticity of colloidal mixtures', *J. Chem. Phys.* **108**, pp. 9893–9904
66. Németh, Z.T., H. Löwen (1998): 'Freezing in finite systems: hard discs in circular cavities', *J. Phys. Condensed Matter* **10**, pp. 6189–6203
67. Németh, Z.T., H. Löwen (1999): 'Freezing and glass transition of hard spheres in cavities', *Phys. Rev E* **59**, pp. 6824–6829
68. Neser, S., C. Bechinger, P. Leiderer, T. Palberg (1997a): 'Finite-Size Effects on the Closest Packing of Hard Spheres', *Phys. Rev. Letters.* **79**, pp. 2348–2351
69. Neser, S.T. Palberg, C. Bechinger, P. Leiderer (1997b): 'Direct observation of a buckling transition during the formation of thin colloidal crystals', *Progr Colloid Polymer Science* **104**, pp. 194–197
70. Ohnesorge, R., H. Löwen, H. Wagner (1991): 'Density-funcional theory of surface melting', *Phys. Rev. A* **43**, pp. 2870–2878
71. Pansu, B., P. Pieranski (1984): 'Structures of thin layers of hard spheres: high pressure limit', *J. Physique* **45**, pp. 331–339
72. Phan, S.-E., W.B. Russel, J. Zhu, P.M. Chaikin (1999): 'Effects of polydispersity on hard sphere crystals', J. Chem. Phys. **108**, pp. 9789–9795
73. Pieranski, P., L. Strzelecki, B. Pansu (1983): 'Thin Colloidal Crystals', *Phys. Rev. Lett.* **50**, pp. 900–902
74. Pronk, S., D. Frenkel (1999): 'Can stacking faults in hard-sphere crystals anneal out spontaneously?' *J. Chem. Phys.* **110**, pp. 4589–4592
75. Pusey, P.N. (1991): 'Colloidal Suspensions'. In: *Liquids, Freezing and the Glass Transition*, ed. by J.P. Hansen, D. Levesque, J. Zinn-Justin (North Holland, Amsterdam), pp. 763–942
76. Reiss, H., H.L. Frisch, E. Helfand, J.L. Lebowitz (1960): 'Aspects of the Statistical Thermodynamics of Real Fluids', *J. Chem. Phys.* **32**, pp. 119–124

77. Rosenfeld, Y. (1996): 'Close-packed configurations, 'symmetry breaking', and the freezing transition in density functional theory', *J. Phys. Condensed Matter* **8**, pp. L795–L801
78. Rosenfeld, Y. , M. Schmidt, H. Löwen, P. Tarazona (1997): 'Fundamental-measure free-energy density functional for hard spheres: Dimensional crossover and freezing', *Physical Review E* **55**, pp. 4245–4263
79. Rosenfeld, Y. (1998): 'Self-consistent density functional theory and the equation of state for simple liquids', *Mol. Phys.* **94**, pp. 929–936
80. Schmidt, M., H. Löwen (1996): 'Freezing between Two and Three Dimensions', *Phys. Rev. Letters* **76**, pp. 4552–4555
81. Schmidt, M., H. Löwen (1997): 'Phase diagram of hard spheres confined between two parallel plates', *Phys. Rev. E* **55**, pp. 7228–7241
82. Sear, R.P. (1998): 'Phase seperation and crystallisation of polydisperse hard spheres', *Europhys. Letters* **44**, pp. 531–535
83. Tonks, L. (1936): 'The Complete Equation of State of One, Two and Three-Dimensional Gases of Hard Elastic Spheres', *Phys. Rev.* **50**, pp. 955–963
84. Truskett, T.M., S. Torquato, S. Sastry, P.G. Debenedetti, F.H. Stillinger (1998): 'Structural precursor to freezing in the hard-disk and hard-sphere system', *Phys. Rev. E* **58**, pp. 3083–3088
85. Van Blaaderen, A. and P. Wiltzius (1995): 'Real-Space Structure of Colloidal Hard-Sphere Glasses', *Science* **270**, pp. 1177–1179
86. Van Winkle, D.H., C.A. Murray (1986): 'Layering transitions in colloidal crystals as observed by diffraction and direct lattice imaging', *Phys. Rev. A* **34** (1986), pp. 562–573
87. Warren, P.B. (1999): 'Fluid-fluid phase seperation in hard spheres with a bimodal size distribution', *Europhys. Letters* **46**, 295–300
88. Weiss, J., D.W. Oxtoby, D.G. Grier, C.A. Murray (1995): 'Martensitic transition in a confined colloidal suspension', *J. Chem. Phys.* **103**, pp. 1180–1190
89. Wyler, D., N. Rivier, H. Frisch (1987): 'Hard-Sphere fluid in infinite dimensions', *Phys. Rev. A* **36**, pp. 2422–2431
90. Xu, H., M. Baus (1992): 'A density functional study of superlattice formation in binary hard-sphere mixtures', *J. Phys. Condensed Matter* **4**, pp. L663–L668